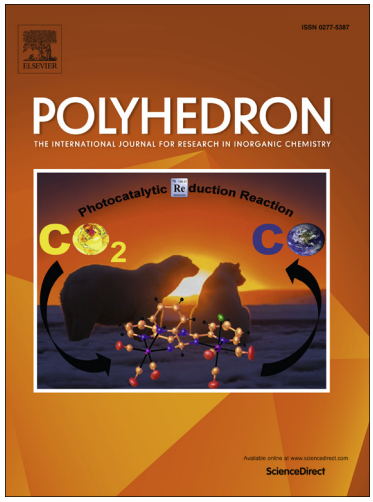

Tetrabromocatecholato Mn(III) Complexes of Bis(phenol) diamine Ligands as Models for Enzyme-Substrate Adducts of Catechol Dioxygenases

Elham Safaei, Leila Hajikhanmirzaei, Saman Alavi, Yong-Ill Lee, Andrzej Wojtczak, Zvonko Jagličić

PII: S0277-5387(16)30338-2
DOI: http://dx.doi.org/10.1016/j.poly.2016.07.041
Reference: POLY 12135

To appear in: *Polyhedron*

Received Date: 14 April 2016
Revised Date: 10 July 2016
Accepted Date: 14 July 2016

Please cite this article as: E. Safaei, L. Hajikhanmirzaei, S. Alavi, Y-I. Lee, A. Wojtczak, Z. Jagličić, Tetrabromocatecholato Mn(III) Complexes of Bis(phenol) diamine Ligands as Models for Enzyme-Substrate Adducts of Catechol Dioxygenases, *Polyhedron* (2016), doi: http://dx.doi.org/10.1016/j.poly.2016.07.041

Tetrabromocatecholato Mn(III) Complexes of Bis(phenol) diamine Ligands as Models for Enzyme-Substrate Adducts of Catechol Dioxygenases

Elham Safaei*[a], Leila Hajikhanmirzaei[b], Saman Alavi[c],

Yong-Ill Lee[d], Andrzej Wojtczak[e], Zvonko Jagličić[f]

[a]*Department of Chemistry, College of Sciences, Shiraz University, Shiraz, 71454, Iran*
[b]*Institute for Advanced Studies in Basic Sciences (IASBS), 45137-66731, Zanjan, Iran*
[c]*Department of Chemistry and Biomolecular Sciences, University of Ottawa, Ottawa, Canada*
[d]Department of Chemistry, Changwon National University, Changwon 641-773, South Korea
[e]Nicolaus Copernicus University, Department of Chemistry, 87-100, Torun, Poland
[f]Institute of Mathematics, Physics and Mechanics & Faculty of Civil and Geodetic Engineering, University of Ljubljana, Jadranska 19. SI-1000, Ljubljana, Slovenia
Correspondence to: Elham Safaei

E-mail:safaei@ iasbs.ac.ir

Abstract

Two mononuclear manganese(III) complexes of bis(phenol) diamine ligands (H_2L^{NEX}) and 2,3,4,5-tetrabromocatechol (TBC), MnL^{NEX}(TBC), were synthesized as models for enzyme-catechol adducts of the intradiol Fe-dependent catechol dioxygenases. X-ray analysis of the complexes has revealed that the manganese center in the model compounds has a distorted octahedral coordination sphere and is surrounded by the L^{NEX} ligand and two oxygen atoms of TBC. The phenolate moieties of MnL^{NEX}(TBC) were electrochemically oxidized to phenoxyl radicals. Consistent with the electrochemical results, quantum chemical calculations showed that the HOMO and LUMO levels on both complexes are on the phenolate moieties. The paramagnetic properties of the manganese(III) center of the complexes have been investigated by magnetic susceptibility measurements. $H_2L^{NEX}/MnCl_2$ showed quite good enzyme-mimicking reactivity. It utilized molecular oxygen in carrying out the cleavage of di-*tert*-butyl catechol at room temperature. To the best of our knowledge this is the second report where a manganese complex can perform oxygenase and not oxidase activity.

Keywords: Catechol dioxygenases; Mn complexes; Model complexes; Bis(phenol) diamine

1. Introduction

Aromatic compounds are among the most prominent environmental pollutants, being introduced by chemical, pharmaceutical, explosive, dyes and agrochemical industries. Since they are very stable due to the delocalization of π orbitals, they accumulate in the soil, water and food chain and cause mutagenic damage. Microorganisms catabolize aromatic compounds by converting them to hydroxylated intermediates and then cleave the benzene nucleus with ring dioxygenases [1]. Catechol dioxygenases contain a mononuclear iron or manganese active center to perform the oxygenative cleavage of the aromatic rings of catechols. These enzymes form a metal-catecholate complex as a reaction intermediate in the catalytic cycles. To explore the mechanisms of the reactions performed by these enzymes, various types of catecholate complexes have been developed with iron or copper, and their reactivity with dioxygen has been studied [2-27].

Intradiol cleaving catechol dioxygenases require Fe(III), while the extradiol cleaving class contains Fe(II) [28]. There are a few examples of extradiol cleaving enzymes containing manganese in their active sites (Scheme 1) [29-33]. Extradiol catechol dioxygenases catalyze the cleavage of dihydroxybenzene rings with the incorporation of both atoms from O_2 to yield muconic semi-aldehyde products [34-36]. The mechanism proposed for extradiol dioxygenases is compatible with the experimental [37-41] and computational [42] studies conducted to date.

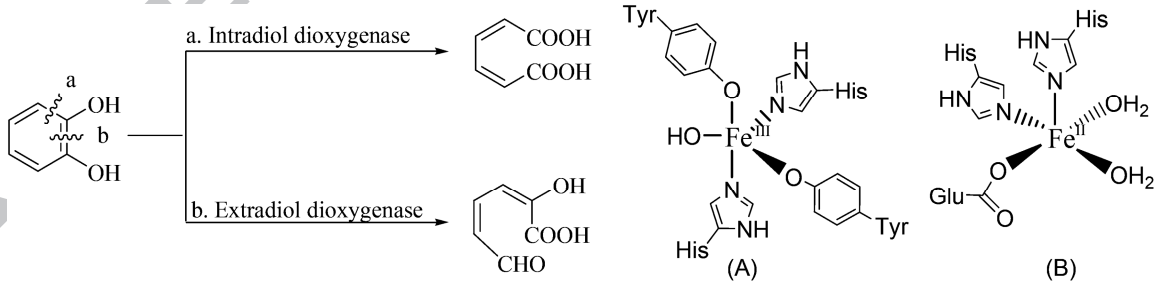

Scheme 1. Modes of catechol cleavage catalyzed by catechol-1,2-dioxygenase (intradiol cleavage) and catechol 2,3-dioxygenase (extradiol cleavage) [26] using oxygenase enzymes (A and B)

The X-ray crystal structure of another extradiol dioxygenase, homoprotocatechuate 2,3-dioxygenase (MndD), isolated from *Arthrobacter globiformis*, has been determined to high resolution by Lipscomb and co-workers[43]. The active-site of this enzyme (Scheme 2) contains a Mn^{2+} metal ion ligated by two equatorial tyrosine and histidine ligands (H214NE1 and E267OE1), one histidine axial ligand (H155NE1) and two to three water molecules. The substrate (2,3-dihydroxyphenylacetate [HPCA]) chelates the metal asymmetrically at sites trans to the two imidazole ligands [43].

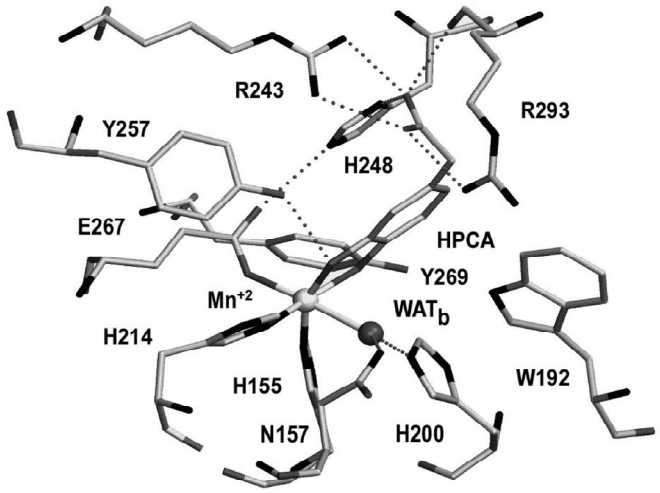

Scheme 2. Diagram of the interaction of the substrate with residues of the active site in MndD. The active-site Mn^{2+} is shown as a light grey sphere, while a single equatorial solvent is shown as a dark sphere [43]

In the present work, the coordination, magnetic and redox properties of new mononuclear manganese(III) complexes of the bis (phenol)diamine ligand H_2L^{NEX} [44] as models for the enzyme-substrate adduct of the intradiol catechol dioxygenase are described (Scheme 3).

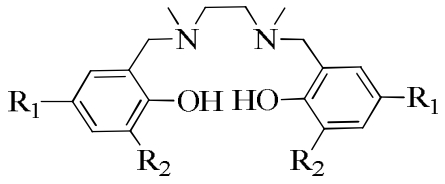

L^{NEC} : $R_1 = R_2 = Cl$

L^{NEB} : $R_1 = R_2 = Br$

Scheme 3. Bis(phenol)diamine ligand H_2L^{NEX} [44]

2. Experimental

2.1. Materials and physical measurements

Reagents or analytical grade materials were obtained from commercial suppliers and used without further purification, except those for electrochemical measurements. Fourier transform infrared spectroscopy on KBr pellets was performed on a FT-IR Bruker Vector 22 instrument. UV-Vis absorbance digitized spectra were collected using a CARY 100 spectrophotometer. Magnetic susceptibility was measured for powder samples of the solid material over the temperature range 2-300 K using a SQUID susceptometer (Quantum Design MPMS-XL-5) at a constant field of 1000 Oe. Voltammetric measurements were made with a computer controlled electrochemical system (ECO Chemie, Utrecht, The Netherlands) equipped with a PGSTA 30 model and driven by GPES (ECO Chemie). A glassy carbon electrode with a surface area of 0.035 cm^2 was used as the working electrode and a platinum wire served as the counter electrode. The reference electrode was an Ag wire as the quasi reference electrode. Ferrocene was added as an internal standard after completion of the experiment set and the potentials are referenced vs. the ferrocenium/ferrocene couple (Fc^+/Fc). Crystals of the MnL^{NEB}(TBC) and MnL^{NEC}(TBC) complexes suitable for the X-ray diffraction experiment were grown from EtOH-CH_2Cl_2 solutions. The X-ray data were collected with an Oxford Sapphire CCD diffractometer using MoKα radiation λ =0.71073 Å, at 293(2) K, by the ω-2θ method. Structures have been solved by direct methods and refined with the full-matrix least-squares method on F^2 with the use of the SHELX97[45] program package. Numerical absorption corrections were applied (RED171 package of programs [46] Oxford Diffraction, 2000). The absolute structures for the complexes were determined with the Flack method [47]. No extinction correction was applied. For both structures, the positions of the hydrogen atoms were found from the electron density maps, and hydrogen atoms were constrained in the refinement.

2.2. Preparation

2.2.1. Synthesis of the MnL^{NEX}(TBC) complexes

To a stirred mixture of H_2L^{NEX} (1.00 mmol) and $MnCl_2$ (0.13 g, 1.00 mmol) in ethanol (50 ml), triethylamine (0.20 g, 2.00 mmol) was added under continuous stirring. After 30 minutes, an ethanol solution of tetrabromocatechol (0.40 g, 1.00 mmol) and triethylamine (0.20 g, 2.00 mmol) was added to the reaction mixture. The reaction mixture was then stirred for 3 h at room temperature. Crystals suitable for X-ray diffraction experiments were obtained by the slow evaporation of a dichloromethane and ethanol mixture.

2.2.1.1. Synthesis of MnL^{NEB}(TBC)

Yield: 0.69 g (70%). Anal. Calcd. for $C_{30}H_{34}Br_8MnN_3O_4$ (1194.82 g/mol): C, 30.13; H, 2.85; N, 3.52%. Found: C, 30.0; H, 2.50; N, 3.41%. IR (KBr, cm^{-1}): 3432, 2987, 2849, 2706, 1579, 1439, 1312, 1231, 1169, 1063, 931, 864, 749, 552, 473. UV-Vis in CH_2Cl_2: λ_{max}, nm (ε, M^{-1} cm^{-1}): 294 (21630), 371(6100).

2.2.1.2. Synthesis of MnL^{NEC}(TBC)

Yield: 0.69 g (70%). Anal. Calcd. for $C_{30}H_{34}Br_4Cl_4MnN_3O_4$ (1016.98 g/mol): C, 35.4; H, 3.34; N, 4.13%. Found: C, 35.1; H, 3.2; N, 4.05%. IR (KBr, cm^{-1}): 3800, 3442, 2978, 1632, 1433, 1312, 1152, 1059, 932, 858, 734, 552. UV-Vis in CH_2Cl_2: λ_{max}, nm (ε, M^{-1} cm^{-1}): 294 (21630), 371(6100).

2.2.2. Catalytic oxidative cleavage of 3,5-di-tert-butyl-catechol by the $MnCl_2/H_2L^{NEB}$ catalytic system

Despite our efforts, the synthesis of the $MnL^{NEX}Cl$ complex from the reaction of $MnCl_2$ and the H_2L^{NEC} ligand and consequent investigation of the catalytic oxidative cleavage of 3,5-di-*tert*-butyl-catechol by this complex was unsuccessful. In the following experiment we used $MnCl_2/H_2L^{NEB}$ as an enzyme mimic catalytic system for cleavage of 3,5-di-*tert*-butyl-catechol.

A solution of $MnCl_2$ (1 mmol) and H_2L^{NEC} (1 mmol) was added to a solution of triethylamine (2 mmol) in 5 ml methanol and (1 mmol) 3,5-di-*tert*-butyl-catechol (3,5-DTBC). The solution was exposed to dioxygen and stirred for 48 h; the violet color slowly changed to dark green. The progress of the reaction was followed by TLC, ^{1}H NMR and mass spectrometry, and they showed the disappearance of 3,5-DTBC. The products were extracted from the aqueous solution with diethyl ether (3 × 30 mL). The organic layer was separated, washed with 2 M HCl (2 × 20 mL), dried over anhydrous Na_2SO_4 at room temperature and then filtered off. The filtrate was evaporated to give the cleavage products in small amounts. The product was quantified by the GC-MS technique. The same experiment was repeated in the absence of $MnCl_2/H_2L^{NEB}$ or H_2L^{NEC}.

2.2.3. Computational methods

The initial structures of the MnL^{NEB}(TBC) and MnL^{NEC}(TBC) complexes in the present work and the FeL^{NEB}(TBC) and FeL^{NEC}(TBC) complexes of our previous studies were extracted from Crystallographic Information Files (CIFs) of the solid phase of these materials [48]. The structures of the complexes were optimized with the Gaussian 09 suite of programs [49] using density functional theory with the unrestricted hybrid B3LYP exchange/correlation functional [50] and the DGDZVP full-electron basis set [51,52]. This level of theory and basis set have been used successfully in computations of Fe(II) complexes and other transition metal complexes [53,54]. The charges of -1 and multiplicities corresponding to high spin complexes ($2S+1 = 5$ for Mn(III) and $2S+1 = 6$ for Fe(III)) were used during the optimization. The spins chosen for the complexes are consistent with the magnetic susceptibility measurements described below.

3. Results and discussion

The H_2L^{NEX} ligands were synthesized from N,N-dimethyl ethylene diamine, formaldehyde and bromine- and chlorine-substituted phenols in a simple Mannich condensation. Since the

formaldehyde used in the reaction contained 63% water, the process was carried out in water instead of methanol, as reported for similar aminophenol ligands.

The H_2L^{NEX} ligands were treated with $MnCl_2$, triethylamine and tetrabromocatechol (TBC) in a suitable ratio and the solution was refluxed to yield the Mn complexes MnL^{NEX}(TBC) with high yield (Scheme 4).

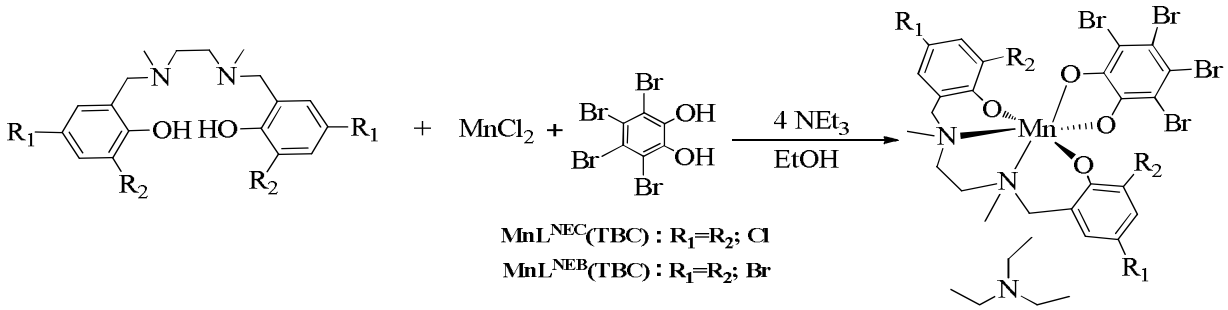

Scheme 4. The reaction pathway for the synthesis of the MnL^{NEX}(TBC) complexes

In the IR spectra of these complexes, the strong and sharp band at 3387 cm^{-1}, corresponding to the ν_{OH} stretch of the ligand (H_2L^{NEX}), was replaced by a broad band, proving the coordination of phenol groups to the metal center. The presence of ligand bands in the IR spectra of the complexes confirms the complexation of the ligand.

The visible spectra of the MnL^{NEX}(TBC) complexes are characterized by two absorption bands. The absorption bands in the lower energy region (around 550 nm) are assigned to ligand-to-metal charge transfer (LMCT) transitions (Figure 1, Table 1). The absorption bands in the higher energy region (around 290 and 370 nm) are caused by $\pi \rightarrow \pi^*$ transitions involving the phenolate and catecholate units.

Figure 1

Table 1

3.1. Description of crystal structures

Both MnL^{NEX}(TBC) complexes crystallize in the non-centrosymmetric orthorhombic space group *Pna*2_1, as determined based on the systematic absences. The X-ray experimental data and structure refinement for the crystal structures are summarized in Table 2. Selected bond lengths and angles are presented in Table 3.

Table 2.

Table 3.

3. 1. 1. X-ray crystal structure of MnL^{NEB}(TBC)

The asymmetric part of the MnL^{NEB}(TBC) structure is formed by the complex monoanion and $(Et)_3NH^+$ cation. Electron density maps have revealed the presence of an H atom bound to the N3 atom of $(Et)_3N$. Therefore, the complex anion contains catecholate dianion and L^{NEB} dianion ligands within the Mn(III) coordination sphere (Figure 2).

Figure 2

In the complex reported here, the coordination sphere of the Mn atom is octahedral with four-dentate L^{NEB} and bi-dentate catecholate ligands. The relative positions of the L^{NEB} phenolate O atoms in the coordination sphere is *cis*. The phenolate O1 and N2 atoms of the L^{NEB} ligand are positioned *trans* relative to the catecholate oxygen atoms. This structure is identical to the organization of the FeL^{NEB}(TBC) complex [55]. Such an architecture resembles that suggested for catechol 1,2-dioxygenases [56], being intradiol oxygenases, despite the fact that those enzymes contain the Fe ion, while a Mn center is found in some extradiol dioxygenases.

The configuration S,S-N1,N2 is found in the molecule constituting the asymmetric unit. However, the presence of a glide plane symmetry in the space group results in the opposite R,R-N1,N2 diastereomers, related by that symmetry. In MnL^{NEB}(TBC), the bond distances within the Mn coordination sphere are similar to those found in the analogous Fe complex [55]. In the complex reported here, the Mn-O bonds formed by the phenolate O1 and O2 atoms of L^{NEB} and O3 and O4

atoms of TBC are shortest, and range from Mn1-O3 1.893(6) to Mn1-O2 2.056(5) Å. In the Fe complex the analogous bond distances formed by the L^{NEB} O1 and O2 atoms were longer by about 0.04 and 0.1 Å. Similar to other investigated complexes of such ligands, the longest distances are found for Mn-N bonds (Table 3), with their distances being almost identical to those reported for the Fe complex. The statistically significant difference in the length of the Mn-O(phenolate) bonds corresponds to the difference reported for the Fe coordination sphere in catechol 1,2-dioxygenase [56]. The Mn1-O3 bond of 1.893(6) Å, positioned trans to the L^{NEB} O1 atom, is significantly shorter than the Mn1-O4 bond of 2.024(5) Å, which is *trans* to N2. That is similar to the results obtained for the FeL^{NEB}(TBC) complex, and the observed non-equivalence is consistent with that expected for the trans effect of the tertiary N1 atom. The observed short Mn1-O3 and Mn1-O1 bonds in the trans positions, when compared to other coordinate bonds in the complex, might be a manifestation of the Jahn-Teller effect for the Mn(III) ion. However, both O atoms belong to phenolate fragments and significant coulombic interactions might be responsible for the observed difference. Such an interpretation is further supported by the analogous effect found for the Fe(III) complexes [55].

The valence geometry of the L^{NEB} ligand is typical for such systems. The C-Br distances range from C2-Br1 of 1.893(7) to C13-Br3 1.922(8) Å. The conformation of the ethylenediamine moiety is synclinal, with the N1-C8-C9-N2 torsion angle being 56.2(11) °, almost identical to that of 56.8(15)° reported for FeL^{NEB}(TBC). The valence geometry of TBC and $(Et)_3NH$ is typical. The C-Br distances in TBC range from C20-Br5 of 1.865(9) to C21-Br6 of 1.902(9) Å.

The dihedral angle between the best planes of the L^{NEB} phenolic rings is 85.9(4) °, identical to that of 85.9° found in the analogous Fe complex. The dihedral angles between phenolic rings C1--C6 and C11--C16 and the TBC ring plane are 82.2(4) and 70.0(4) °, similar to the corresponding angles of 83.5 and 69.0 ° reported for the FeL^{NEB}(TBC) complex [55].

The conformation of the chelate ring Mn1-O3-C19-C24-O4, formed by the catecholate, is twisted on O4-Mn1. The Mn1-N1-C8-C8-N2 ring is an envelope on the C9 atom, the Mn1-O1-C1-C6-C7-N1 ring is a screw-boat, while the Mn1-O2-C16-C11-C10-N2 ring is an envelope.

Crystal packing analysis revealed the presence of an intramolecular H-bond, N3-H3N…O4, the N…O distance being 2.937(9) Å. Several C-H…O and C-H-Br interactions were also found, the details of which are presented in Table 4.

Table 4.

3. 1. 2. X-ray crystal structure of MnL^{NEC}(TBC)

The asymmetric part of the MnL^{NEC}(TBC) structure consists of a complex monoanion and $(Et)_3NH^+$ cation. Electron density maps have revealed the presence of an H atom bound to the N3 atom of $(Et)_3N$. The complex anion contains a catecholate dianion and L^{NEC} dianion ligands within the Mn(III) coordination sphere (Figure 3).

Figure 3

In the reported complex, the coordination sphere of the Mn atom is octahedral with the four-dentate L^{NEC} and bi-dentate catecholate ligands. The relative positions of the L^{NEC} phenolate O atoms in the coordination sphere are *cis*. The L^{NEC} O2 and N1 atoms are positioned trans. The phenolate O1 and N2 atoms of the L^{NEC} ligand are positioned *trans* relative to the catecholate O3 and O4 atoms, respectively. That is identical to the organization of MnL^{NEC}(TBC) reported here and the FeL^{NEC}(TBC) complex [55]. Similar to MnLNEB(TBC), the Mn1-O1 and Mn1-O3 bonds involving the phenolate group are the shortest in the coordination sphere of the Mn atom. Such an architecture resembles that suggested for the active site of the intradiol catechol 1,2-dioxygenases containing Fe and not Mn [56].

The configuration S,S-N1,N2 is found in the molecule constituting the asymmetric unit. Since glide planes are present in the space group, symmetry related complex molecules occur as the opposite R,R-N1,N2 diastereomers. In MnL^{NEC}(TBC), the O1 atom of L^{NEC} positioned *trans* to the TBC O3

atom forms an Mn1-O1 bond of 1.898(4) Å, which is significantly shorter than the Mn1-O2 bond, 2.023(4) Å, formed by the oxygen atom positioned trans to the N1 atom of L^{NEC}. On the other hand, the trans effect of the L^{NEC} N2 atom results in the Mn1-O4 bond, 2.039(4) Å, being significantly longer than the Mn1-O3 bond, 1.881(4) Å (Table 3). Such an effect is consistent with the geometry of the coordination sphere found in both MnL^{NEB}(TBC) and FeL^{NEC}(TBC) [55]. The statistically significant difference in the length of the Mn-O(TBC) bonds corresponds to the difference reported for the Fe coordination sphere in catechol 1,2-dioxygenase and is consistent with the mechanism proposed for 3,4-PCD [56].

The valence geometry of the L^{NEC} ligand is typical for such a system and is similar to that reported for FeL^{NEC}(TBC) [55]. The C-Cl distances range from C15-Cl4 of 1.735(7) to C13-Cl3 of 1.779(7) Å. The conformation of the ethylenediamine moiety is synclinal, with an N1-C8-C9-N2 torsion angle of 59.4(7) º, similar to the 56.2(11) º found for MnL^{NEB}(TBC), or that of -57.1(5) º reported for the opposite diastereoisomer in FeL^{NEC}(TBC) [55]. The valence geometries of TBC and $(Et)_3NH$ are typical. For TBC, the C-Br distances range from C22-Br3 of 1.874(6) to C21-Br2 of 1.899(7) Å.

The dihedral angle between the best planes of the L^{NEC} phenolic rings is 86.6(3) º, very similar to that of 85.9 º found in the Fe complex. The dihedral angles between the phenolic rings C1--C6 and C11--C16 and the TBC ring plane are 82.8(3) and 72.4(3) º, the values are similar to the corresponding angles found for MnL^{NEB}(TBC) or 87.5, 72.1 and 83.2 º reported for the FeL^{NEC}(TBC) complex [55].

The Mn1-O3-C19-C24-O4 chelate ring formed by the catecholate is flat, with the atom deviations from the best plane not exceeding 0.042(2) Å. The Mn1-N1-C8-C8-N2 ring has a conformation of an envelope on the C9 atom, the Mn1-O1-C1-C6-C7-N1 ring is a screw-boat, and the Mn1-O2-C16-C11-C10-N2 ring has an envelope conformation.

Analysis of the crystal packing revealed the presence of an intermolecular H-bond, N3-H1N...O4[x,y,1+z] with an N…O distance of 2.916(6) Å. Intramolecular C-H…O and C-H…Br

interactions, as well as intermolecular C-H…O and C-H…Cl interactions are also found, details of which are presented in Table 5.

Table 5

3.2. Magnetic susceptibility measurements

The susceptibilities of the two samples increase with decreasing temperature. The analysis of the susceptibility χ(T) was performed by applying the Curie-Weiss law, $\chi = \frac{C}{(T-\theta)}$, for T > 50 K, which gives us information on the magnitude of magnetic moments through the Curie-Weiss constant *C* corresponding to the expected values for Mn(III) ions in both complexes [57,58]. The magnetic susceptibilities of the two samples are shown in Figure 4. The Curie-Weiss constants *C* are 3.03 and 2.89 emu/mol respectively. The magnitudes of effective magnetic moments of 4.92 and 4.80 μ_B of the complexes at r.t. (Tables 1s and 2s) are very close to the spin only value of 4.9 μ_B, expected for a high spin magnetically dilute d^4 manganese(III) ion, indicating little or no antiferromagnetic interaction [59].

Figure 4

Table 6

3.3. Electrochemistry

The cyclic voltammograms of the MnL^{NEB}(TBC) complex show the redox process is possibly associated with the TBC/TBSQ and phenolate/phenoxyl couples in the complexes [60,61], but we do not have any evidence for that. The cyclic voltammogram of MnL^{NEB}(TBC) recorded in the range -0.3-0.3 V in CH_2Cl_2 showed one quasi-reversible redox wave versus Ag/AgCl (*E*=0.09V) (Figures 5 and 6).

Figure 5

Figure 6

3.4. $MnCl_2/H_2L^{NEB}$ catalyzed oxygenation of catechol

The focus of this experimental part was to catalyze the oxidative cleavage of 3,5-DTBC with dioxygen as the oxidant. In the presence of 5% of the catalyst, 100% of 3,5-di-*tert*-butyl-catechol (3,5-DTBC) was selectively converted to one cleavage product A (Scheme 5). The progress of the reaction was followed by ^{1}H NMR spectroscopy. The signals of 3,5-DTBC (δ 6.90, 1.37 and 1.23 ppm) disappeared without the appearance of signals for the 3,5-di-*tert*-butyl-cquinone, 3,5-DTBQ (δ 6.93, 6.22, 1.28 and 1.23 ppm) [62].

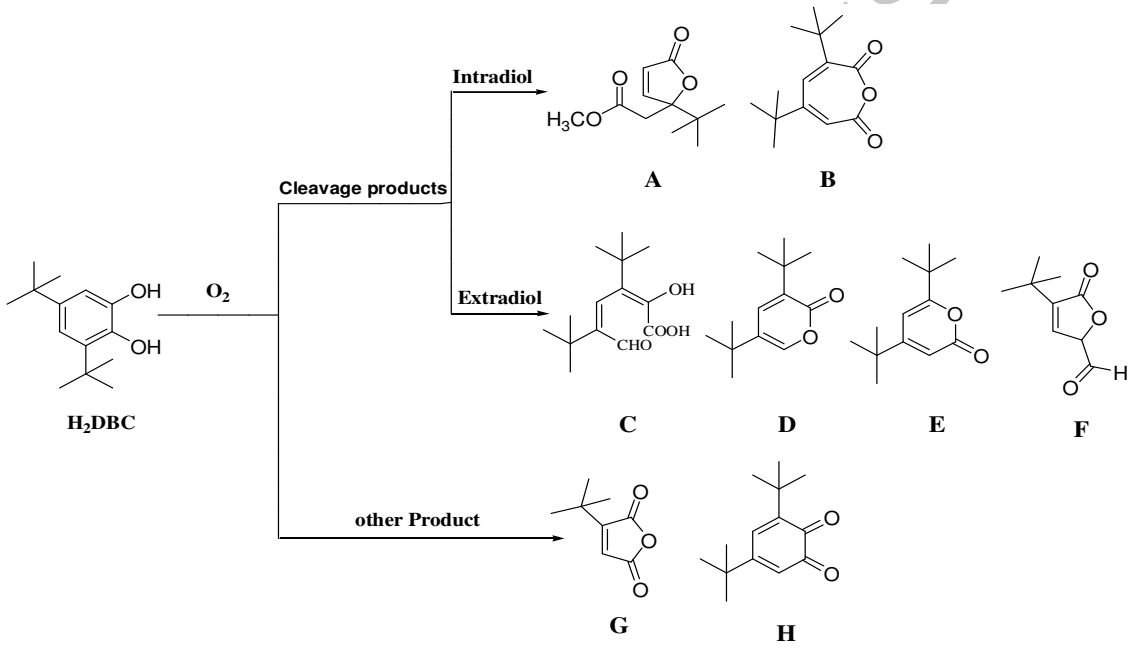

Scheme 5. Products of catechol cleavage catalyzed by catechol dioxygenases and their models [22]

This observation was in contrast to our previous results for the same reaction catalyzed by $L^{Gly}Fe$ [62], in which 3,5-DTBC was oxidized to produce 3,5-di-*tert*-butyl-*o*-benzoquinone (3,5-DTBQ) or different cleavage oxidation products of catechols using the FeL^{GDC} complex [63] or other catalysts [64-66]. It is worth noting that in both blank tests, in the absence of $MnCl_2/H_2L^{NEB}$ or H_2L^{NEC}, no oxidation or oxygenation products of 3,5-DTBC were observed. This criterion is attributed to the Lewis acidity of the metal center in the $MnCl_2/H_2L^{NEB}$ catalyst system which facilitates the oxidative

cleavage of catechol. The progress of the reaction was followed by GC-mass spectrometry. GC-MS technique was used to identify and quantify the oxidative cleavage product of 3,5-DTBC, and this indicated the conversion of 3,5-DTBC to only product "**A**". Finally, the results showed that the $MnCl_2/H_2L^{NEB}$ catalyst system can act as a good catalyst for the cleavage oxygenation of 3,5-DTBC in the presence of oxygen. The oxidative cleavage reaction of catechol with this complex was performed and the results are shown in Figure 7 and Table 7.

Figure 7.

Table 7.

We propose a mechanism based on the tendency of the metal center for 3,5-DTBC binding in the coordination site. Then, electron density is transferred from the aromatic substrate to the Mn(III) center, producing a Mn(II)-DTBSQ species (DTBSQ stands for 3,5-di-*tert*-butyl-*o*-semibenzoquinone). Subsequently, coordination of O_2 to this metal center and further electron transfer from Mn(II)-DTBSQ to O_2 finally produces •O-O-Mn(III)-DTBSQ with O_2 and DTBSQ radical character. As a result the Mn(III) complex plays a role in activating O_2 and catechol, producing species with radical character, which subsequently react with each other. The attack of the bound superoxide on the oxidized catecholate ring would yield an intermediate alkylperoxy species. This intermediate would then rearrange with OOO bond cleavage and ring insertion to produce an intermediate lactone that is hydrolyzed to complete the reaction [67]. Since, the intermediates were unstable, we could not characterize them, and these mechanistic proposals have not received strong support. The role of ligand could be in the tuning of the redox potential of the Mn(III) center for binding of oxygen and catechol.

3.5. Computational results

The Cartesian coordinates of the optimized structures of MnL^{NEB}(TBC) and MnL^{NEC}(TBC) in the present work, together with FeL^{NEB}(TBC) and FeL^{NEC}(TBC), are given in the Supporting

Information. The HOMO-LUMO gaps were determined for each optimized structure and are given in Table 8. Representations of these orbitals are generated using the Avogadro visualization program [64] and are shown in Figure 8. In all the complexes, the HOMO and LUMO are localized on the L^{NEX} molecules and not on the TBC moiety. The location of the HOMO is consistent with the experimental observation that oxidation occurs on the L^{NEX} moiety to give a phenoxyl radical.

Table 8.

Figure 8.

4. Conclusion

Mononuclear manganese(III) complexes of four-dentate N_2O_2 bis(phenol)diamine ligands (H_2L^{NEX}) and 2,3,4,5-tetrabromocatechol, TBC (MnL^{NEX}(TBC)) were synthesized as new models for enzyme-catechol adducts of Fe-dependent intradiol catechol dioxygenases. X-ray analysis of the complexes has revealed that the manganese(III) core in the model compounds have a distorted octahedral coordination sphere and are surrounded by the ligand and two oxygen atoms of TBC. The redox process of MnL^{NEX}(TBC) yielded the corresponding phenoxyl radical species during the cyclic voltammetry experiments.

Variable temperature magnetic susceptibility measurements indicate that the MnL^{NEX}(TBC) complexes are paramagnetic high spin Mn(III) complexes in almost the entire investigated temperature range. Electrochemical measurements and quantum chemical calculations suggest that ionization of the complexes converts the phenolate moieties of the complexes to phenoxy radicals. Our results show that the $MnCl_2/H_2L^{NEB}$ system can act as a good catalyst for the cleavage oxygenation of 3,5-DTBC in the presence of oxygen. Mn dependent catechol dioxygenases contain the Mn(II) ion in the active site, and are bound to a 2His1CO2 triad. They perform extradiol cleavage. The coordination sphere and regioselectivity in catechol cleavage by the present compounds is instead more reminiscent of intradiol cleavage enzymes that employ Fe(III) ions, have

two tyrosine residues in the coordination sphere and perform intradiol cleavage. We suppose that the Mn(III) complex plays a role in activating O_2 and catechol, producing species with radical character which subsequently react with each other, leading to the oxygenative cleavage of catechol .

Appendix A. The structural data for MnL^{NEB}(TBC) and MnL^{NEC}(TBC) have been deposited with the Cambridge Crystallographic Data Centre, the deposition numbers being CCDC 1061488 and 1061489 respectively. This data can be obtained free of charge via http://www.ccdc.cam.ac.uk/conts/retrieving.html, or from the Cambridge Crystallographic Data Centre, 12 Union Road, Cambridge CB2 1EZ, UK; fax: (+44) 1223-336-033; or e-mail: deposit@ccdc.cam.ac.uk.

Acknowledgments

The authors are grateful to the Institute for Advanced Studies in Basic Sciences (IASBS), and also to Changwon, Ljubljana, Nicolaus Copernicus and Ottawa Universities for their valuable help. E. Safaei gratefully acknowledges the support from the Institute for Advanced Studies in Basic Sciences (IASBS) Research Council under Grant No. G2015IASBS127. Yong-Ill Lee acknowledges support from the Priority Research Centers Program (NRF 2010-0029634) through the National Research Foundation of Korea (NRF).

References

[1] T. B. Karegoudar, C. K. Kim, J. Microbiology. 38 (2000) 53-61.

[2] M. Velusamy, M. Palaniandavar, R. S. Gopalan, G. Y. U. Kulkarni, Inorg. Chem. 42 (2003) 8283-8293.

[3] T. D. H. Bugg, C. J. Winfield, Nat. Prod. Rep. 15 (1998) 513–530.

[4] K. Sundaravel, M. Sankaralingam, M. Palaniandavar, E. Suresh, Dalton Trans. (2011) 8444-8458.

[5] M. Costas, M. P. Mehn, M. P. Jensen, L. Jr. Que, Chem. Rev. 104 (2004) 939-986.

[6] E. A. Lewis, W. B. Tolman, Chem. Rev. 104 (2004) 1047-1076.

[7] P. Halder, S. Paria, T. K. Paine, Chem. Eur. J. (2012) 5843-5853.

[8] R. Yamahara, S. Ogo, H. Masuda, Y. Watanabe, J. Inorg. Biochem. 88 (2002) 284-294.

[9] M. Kodera, T. Kawata, K. Kano, Y. Tachi, S. Itoh, S. Kojo, Bull. Chem. Soc. Jpn. 76 (2003) 1957-1964.

[10] K. Selmeczi, M. Reglier, M. Giorgi, G. Speier, Coord. Chem. Rev. 245 (2003) 191-201.

[11] J. Ackermann, F. Meyer, E. Kaifer, H. Pritzkow, Chem. Eur. J. 8 (2002) 247-258.

[12] C. Belle, C. Beguin, I. Gautier-Luneau, S. Hamman, C. Philouze, J. L. Pierre, F. Thomas, S. Torelli, E. Saint-Aman, M. Bonin, Inorg. Chem. 41 (2002) 479-491.

[13] A. Neves, L. M. Rossi, A. J. Bortoluzzi, B. Szpoganicz, C. Wiezbicki, E. Schwingel, Inorg. Chem. 41 (2002) 1788-1794.

[14] J. Kaizer, J. Pap, G. Speier, L. Parkanyi, L. Korecz, A. Rockenbaur, J. Inorg. Biochem. 91 (2002) 190-198.

[15] G. Speier, Z. Tyeklar, P. Toth, E. Speier, S. Tisza, A. Rockenbauer, A. M. Whalen, N. Alkire, C. G. Pierpont, Inorg. Chem. 40 (2001) 5653-5659.

[16] S. Torelli, C. Belle, I. Gautier-Luneau, J. L. Pierre, E. Saint-Aman, J. M. Latour, L. Le Pape, D. Luneau, Inorg. Chem. 39 (2000) 3526-3536.

[17] L. M. Berreau, S. Mahapatra, J. A. Halfen, R. P. Houser, V. G. Young Jr, W. B. Tolman, Angew. Chem. Int. Ed. 38 (1999) 207-210.

[18] R. Mayilmurugan, K. Visvaganesan, E. Suresh, M. Palaniandavar, Inorg. Chem. 48 (2009) 8771-8783.

[19] M. E. Alberto, Chem. Commun. 51 (2015) 8369-8372.

[20] M. R. Malachowski, H. B. Huynh, L. J. Tomlinson, R. S. Kelly, J. W. Furbee Jr, J. Chem. Soc., Dalton Trans. (1995) 31-36.

[21] J. Balla, T. Kiss, R. F. Jameson, Inorg. Chem. 31 (1992) 58-62.

[22] M. Balamurugan, P. Vadivelu, M. Palaniandavar, Dalton Trans. 43 (2014) 14653-14668.

[23] G M. S. Shongwe, C. H. Kaschula, M. S. Adsetts, E. W. Ainscough, A. M. Brodie, M. J. Morris, Inorg. Chem. 44 (2005) 3070-3079.

[24] K. Sundaravel, M. Sankaralingam, M. Palaniandavar, E. Suresh, Dalton Trans. (2011) 8444-8458.

[25] L. Que Jr., M. F. Reynolds, in: A. Sigel, H. Sigel (Eds.), Metal Ions in Biological Systems, vol. 37, Marcel Dekker, New York, 2000, p. 505.

[26] K. Sundaravel, E. Suresh, K. Saminathan, M. Palaniandavar, Dalton Trans. 43 (2014) 14653-14668.

[27] A. K. Whiting, Y. R. Boldt, M. P. Hendrich, L. P. Wackett, L. Que Jr., Biochemistry 35 (1996) 160-170.

[28] M. S. Shongwe, C. H. Kaschula, M. S. Adsetts, E. W. Ainscough, A. M. Brodie, M. J. Morris, Inorg. Chem. 44 (2005) 3070-3079.

[29] J. D. Lipscomb, A. M. Orville, in: A. Sigel, H. Sigel (Eds.), Metal Ions in Biological Systems, vol. 28, Marcel Dekker, New York, 1992, p. 243.

[30] T. Senda, K. Sygiyama, H. Narita, T. Yamamoto, K. Kimbara, M. Fukuda, M. Sato, K. Yano, Y. Mitsui, J. Mol. Biol. 255 (1996) 735-752.

[31] D. H. Ohlendorf, J. D. Lipscomb, P. C. Weber, Nature (London) 336 (1988) 403-405.

[32] L. Que Jr., in: T.M. Loehr (Ed.), Iron Carriers and Iron Proteins, VCH, New York, 1989, pp. 373-466.

[33] M. W. Vetting, L. P. Wackett, L. Que Jr., J. D. Lipscomb, D. H. Ohlendorf, J. Bacteriol. 186 (2004) 1945-1958.

[34] J. D. Lipscomb, A.M. Orville, Metal Ions Biol. Syst. 28 (1992) 243-298.

[35] M. Costas, M. P., Mehn, M. P. Jensen, L. Que Jr, Chem. Rev. 104 (2004) 939-986.

[36] F. H. Vaillancourt, J. T. Bolin, L. D. Eltis, Crit. Rev. Biochem. Mol. Biol. 41 (2006) 241-267.

[37] R. Mayilmurugan, M. Sankaralingam, M. Palaniandavar, Dalton Trans. (2010) 9611-9625.

[38] S. L. Groce, M. A. Miller-Rodeberg, J. D. Lipscomb, Biochemistry 43 (2004) 15141-15153.

[39] E. G. Kovaleva, J. D. Lipscomb, Science 316 (2007) 453-457.

[40] D. M. Arciero, A. M. Orville, J. D. Lipscomb, J. Biol. Chem. 260 (1985) 14035-14044.

[41] S. L. Groce, J. D. Lipscomb, Biochemistry 44 (2005) 7175-7188.

[42] A. Bassan, T. Borowski, P. E. M. Siegbahn, Dalton Trans. (2004) 3153-3162.

[43] M. W. Vetting, L. P. Wackett, L. Que, Jr., J. D. Lipscomb, D. H. Ohlendorf, J. Bacteriol., 186 (2004) 1945-1958.

[44] T. Karimpour, E. Safaei, A. Wojtczak, Z. Jaglicic, A. Kozakiewicz, Inorg. Chim. Acta 395 (2013) 124-134.

[45] G. Sheldrick, Acta Crystallogr., Sect. A 64 (2008) 112-122.

[46] CrysAlis CCD171 and RED171 package of programs, Oxford Diffraction, 2000.

[47] H. D. Flack, Acta Crystallogr., Sect. A 39 (1983) 876-881.

[48] T. Karimpour, E. Safaei, A. Wojtczak, Z. Jaglicic. Inorg. Chim. Acta 405 (2013) 309-317.

[49] Gaussian 09, Revision E.01, M. J. Frisch,; G. W. Trucks, H. B. Schlegel,; G. E. Scuseria, M. A. Robb, J. R. Cheeseman, G. Scalmani, V. Barone, B. Mennucci, G. A. Petersson, H. Nakatsuji, M.

Caricato, X. Li, H. P. Hratchian, A. F.Izmaylov, J. Bloino, G. Zheng, J. L. Sonnenberg, M. Hada, M. Ehara, K. Toyota, R. Fukuda, J. Hasegawa, M. Ishida, T. Nakajima, Y. Honda, O. Kitao, H. Nakai, T. Vreven, J. A. Montgomery, J. E. Peralta, F. Ogliaro, M.Bearpark, J. J. Heyd, E. Brothers, K. N. Kudin, V. N. Staroverov, R. Kobayashi, J. Normand, K. Raghavachari, A. Rendell, J. C. Burant, S. S. Iyengar, J. Tomasi, M. Cossi, N. Rega, J. M. Millam, M. Klene, J. E. Knox, J. B. Cross, V. Bakken, C. Adamo, J. Jaramillo, R. Gomperts, R. E. Stratmann, O. Yazyev, A. J. Austin, R. Cammi, C. Pomelli, J. W. Ochterski, R. L. Martin, K. Morokuma, V. G. Zakrzewski, G. A. Voth, P. Salvador, , J. J. Dannenberg, S. Dapprich, A. D. Daniels, Ö. Farkas, J. B. Foresman, J. V. Ortiz, J. Cioslowski, D. J. Fox, Gaussian, Inc., Wallingford CT, 2009.

[50] A. D. Becke, J. Chem. Phys. 98 (1993), 5648-5652.

[51] N. Godbout, D. R. Salahub, J. Andzelm, E. Wimmer Can. J. Chem. 70 (1992), 560-571.

[52] H. Cheng, B. Djukic, H. A. Jenkins, S. I. Gorelsky, M. T. Lemaire, Can. J. Chem. 88 (2010) 954-963.

[53] C. Sosa, J. Andzelm, B. C. Elkin, E. Wimmer, K. D. Dobbs, D. A. Dixon, J. Phys. Chem. 96 (1992) 6630-6636.

[54] L. Qui, J. G. Lin, X. D. Gong, X. H. Ju, S. N. Luo, Bull. Korean Chem. Soc. 32 (2011) 2358.

[55] D. Moonshiram, I. Alperovich, J. J. Concepcion, T. J. Meyer, Y. Pushkar, Proc. Nat. Acad. Sci. USA, 110 (2013) 3765-3770.

[56] M. P. Valley, C. Kent Brown, D. L. Burk, M. W. Vetting, D. H. Ohlendorf, J. D. Lipscomb, Biochemistry 44 (2005) 11024-11039.

[57] L. Dutta, A. Syamal, Elements of Magnetochemistry, Affiliated East-West Press PVT LTD, 1993, 6-11.

[58] C. Kittel, Introduction to Solid State Physics (8th Ed), John Wiley & Sons, 2005.

[59] M.R. Bermejo, M. Fondo, A. Garcia-Deibe, A.M. Gonzalez, A. Sousa, J. Sanmartin, C.A. McAuliffe, R.G. Pritchard, M. Watkinson, V. Lukov, Inorg. Chim. Acta 293 (1999) 210-217.

[60] S. E. Balaghi, E. Safaei, L. Chiang, E. W. Wong, D. Savard, R. M. Clarke, T. Storr, Dalton Trans. 42 (2013) 6829-6839.

[61] Z. Alaji, E. Safaei, L. Chiang, R. M. Clarke, C. Mu, T. Storr, Eur. J. Inorg. Chem. (2014) 6066-6074.

[62] E. Safaei, H. Sheykhi, A. Wojtczak, Z. Jaglicic, A. Kozakiewicz, Polyhedron 30 (2011) 1219-1224.

[63] I. Saberikia, E. Safaei, M.H. Kowsari, Y. I. Lee, P. Cotic, G. Bruno, H.A. Rudbari, J. Mol. Struct. 1029 (2012) 60-67.

[64] G. Lin, G. Reid, T. D. H. Bugg, J. Am. Chem. Soc. 123 (2001) 5030-5039.

[65] G. Lin, G. Reid, T. D. H. Bugg, J. Chem. Soc. Chem. Commun. (2000) 1119-1120.

[66] M. D. Hanwell, D. E. Curtis, D. C. Lonie, T. Vandermeersch, E. Zurek and G. R. Hutchison, J. Cheminformatics 4 (2012) 1-17.

[67] L. Que, R. Y. N. Ho, Chem. Rev. 96 (1996) 2607-2624.

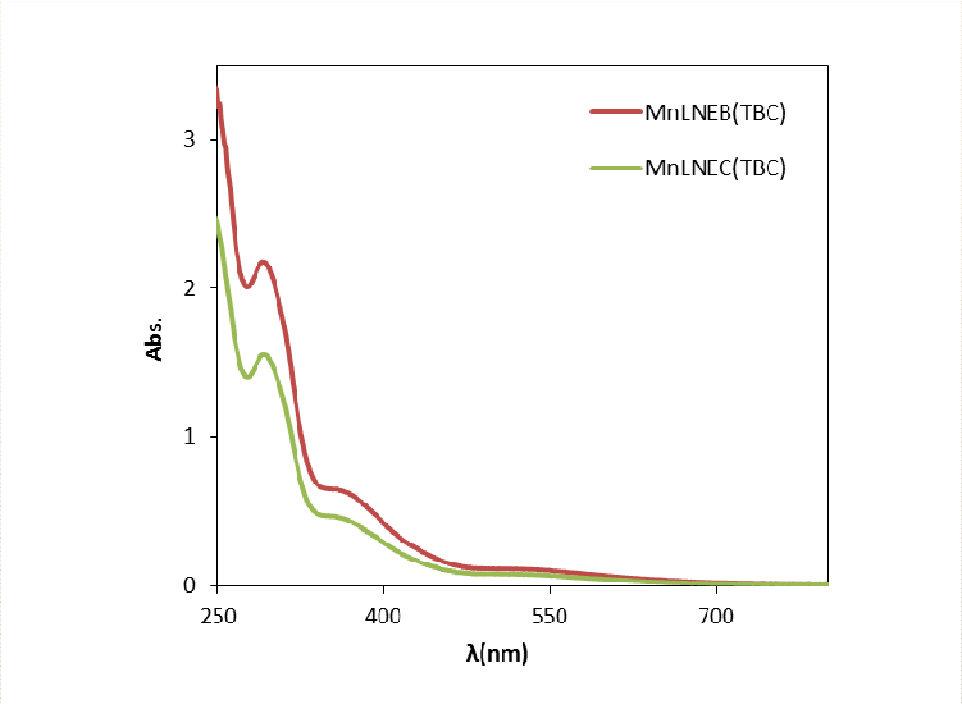

Figure 1. Electronic absorption spectra of **MnL^{NEX}(TBC)** in (1.0×10^{-4} M) CH_2Cl_2 solution

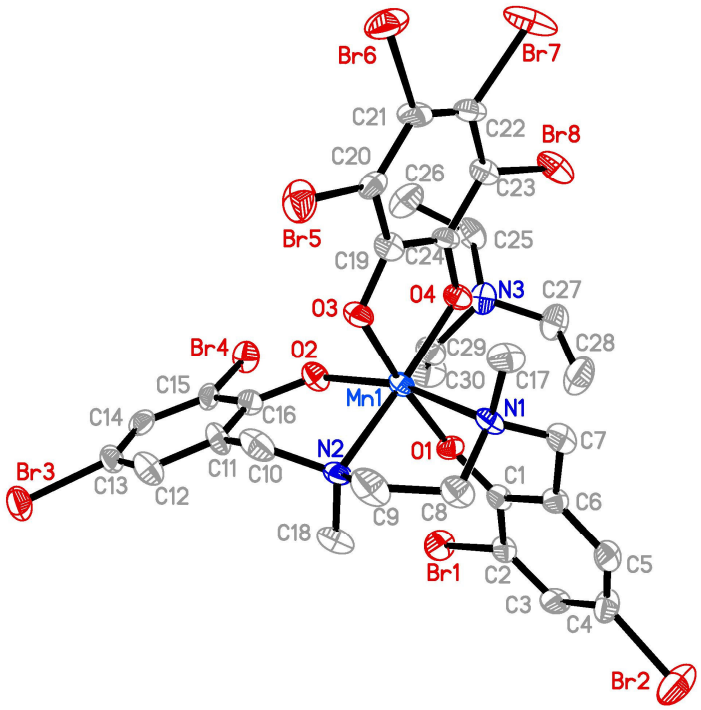

Figure 2. ORTEP diagram and atom labelling scheme for the complex MnL^{NEB}(TBC) Hydrogen atoms are omitted for clarity. Ellipsoids are plotted at the 30% probability level

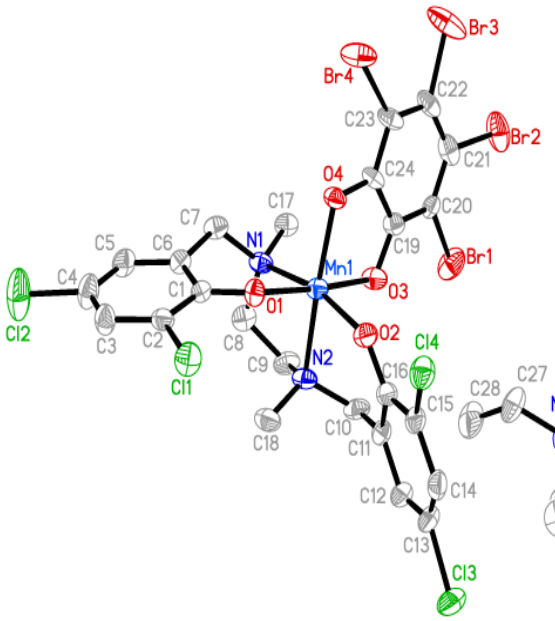

Figure 3. ORTEP diagram and atom labelling scheme for the complex MnL^{NEC}(TBC) Hydrogen atoms are omitted for clarity. Ellipsoids are plotted at the 30% probability level.

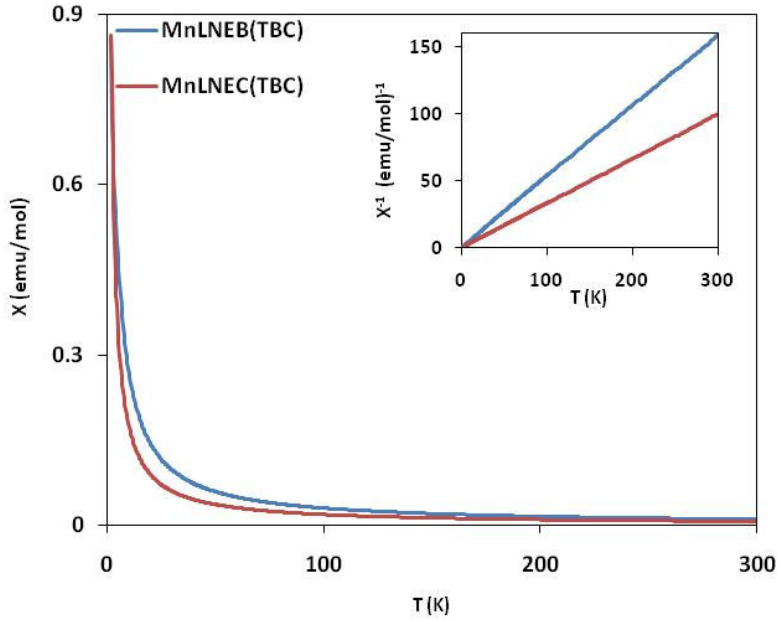

Figure 4. Temperature dependence of susceptibility $\chi(T)$ and μ_{eff} (μB) of MnL^{NEX}(TBC) measured in a magnetic field of H = 1000 Oe

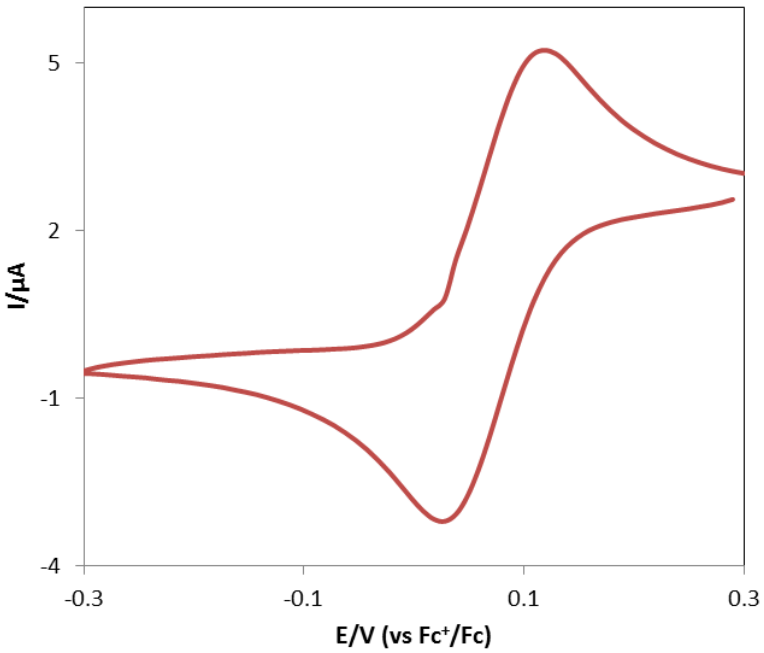

Figure 5. Cyclic voltammogram of MnL^{NEB}(TBC) in CH_2Cl_2 at -80 °C (sc 100 mV s^{-1}).

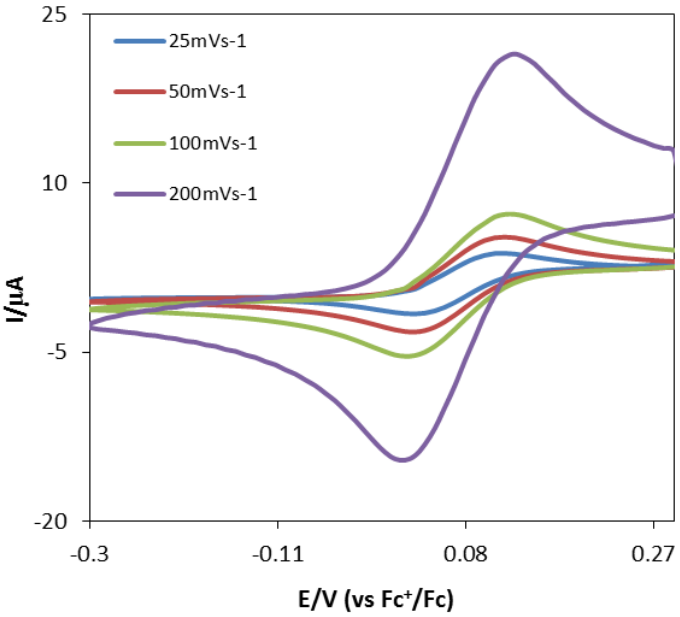

Figure 6. Cyclic voltammogram of MnL^{NEB}(TBC) in CH_2Cl_2 at -80 °C (sc 25-800 mV s^{-1}).

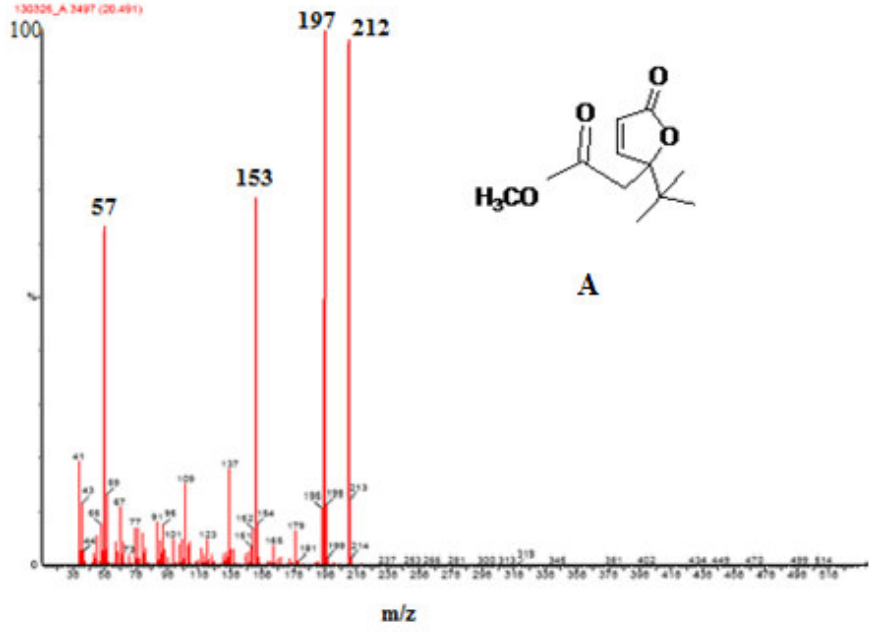

Figure 7. Oxygenative cleavage product of DTBC by $MnCl_2$/ H_2L^{NEC} System monitored by GC/mass spectrometry

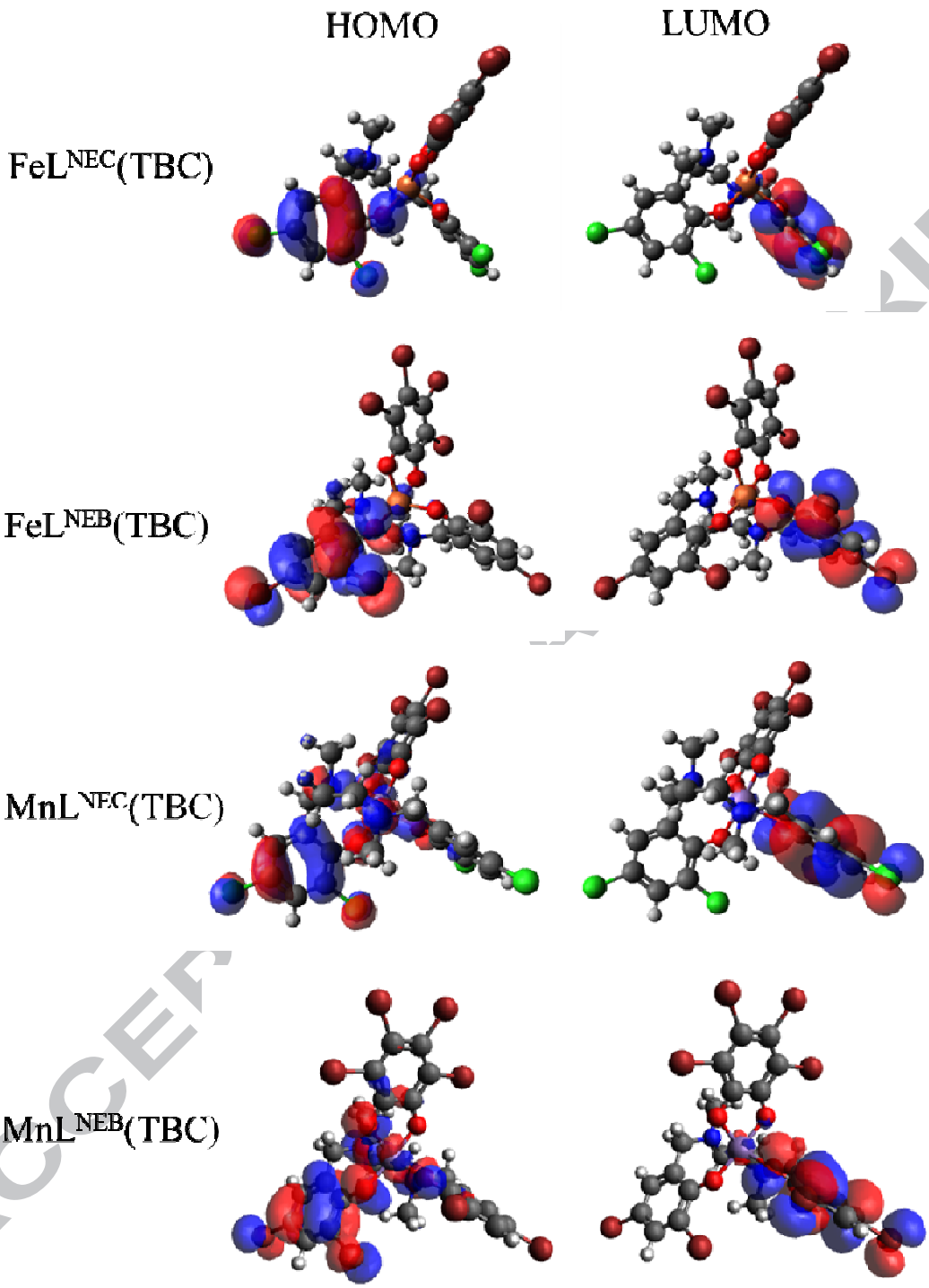

Figure 8. The HOMO and LUMO of the isolated FeL^{NEX}(TBC) and MnL^{NEX}(TBC) complexes

Tetrabromocatecholato Mn(III) Complexes of Bis(phenol) diamine Ligands as Models for Enzyme-Substrate Adducts of Catechol Dioxygenases

Mononuclear manganese(III) and (IV) complexes of four-dentate N_2O_2 bis(phenol)diamine ligands, H_2L^{NEX}, and tetrabromocatechol were synthesized as new models for enzyme-catechol adducts of catechol dioxygenases. The $H_2L^{NEX}/MnCl_2$ enzyme mimicking system utilized molecular oxygen in carrying out the oxidative cleavage of di-*tert*-butyl catechol at room temperature.

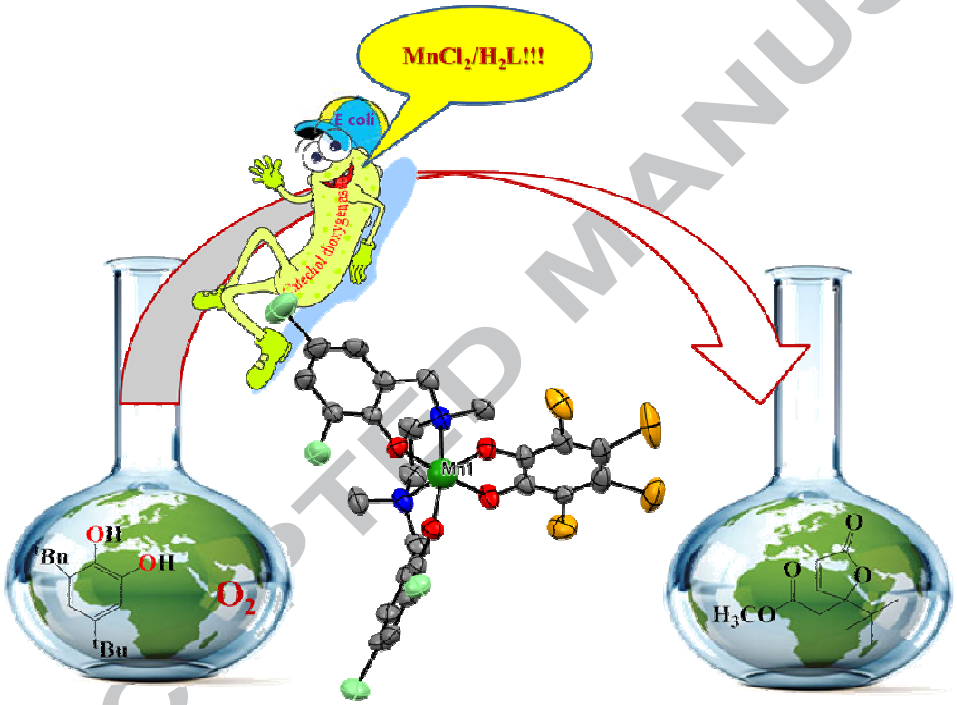

Table 1. The adsorption maximum λmax / nm (ε / M^{-1} cm^{-1}) for the ILCT and LMCT bands of the MnL^{NEX}(TBC) complexes at 1.0×10^{-4} M in CH_2Cl_2 solutions.

MnL^{NEX}(TBC)	λ_{max} / nm(ε / M^{-1} cm^{-1})	λ_{max}/nm(ε /M^{-1} cm^{-1})	λ_{max}/nm(ε /M^{-1} cm^{-1})
MnL^{NEB}(TBC)	294 (21630)	371 (6100)	_
MnL^{NEC}(TBC)	295 (15430)	365 (4520)	527 (760)

Table 2. Crystal data and structure refinement for MnL^{NEX}(TBC)

	MnL^{NEC}(TBC)	**MnL^{NEB}(TBC)**
Empirical formula	$C_{30}H_{34}Br_4Cl_4MnN_3O_4$	$C_{30}H_{34}Br_8MnN_3O_4$
Formula weight	1016.98	1194.82
Temperature, K	293(2)	293(2)
Wavelength, Å	0.71073	0.71073
Crystal system, space group	Orthorhombic, Pna2(1)	Orthorhombic, Pna2(1)
Unit cell dimensions, Å	a = 16.6955(8)	a = 16.8763(10)
	b = 21.1326(12)	b = 21.2881(17)
	c = 10.3371(5)	c = 10.3655(7)
Volume, $Å^3$	3647.1(3)	3723.9(5)
Z, Calculated density, Mg/m^3	4, 1.852	4, 2.131
Absorption coefficient, mm^{-1}	5.077	8.977
F(000)	2000	2288
Crystal size, mm	0.35 x 0.21 x 0.07	0.56 x 0.34 x 0.13
Theta range for data collection, deg	2.19 to 28.40	2.50 to 28.26
Limiting indices	-21≤ h ≤20, -26 ≤ k ≤27, -13≤ l ≤13	-18 ≤ h ≤20, -27 ≤ k ≤27, -12 ≤ l ≤ 12
Reflections collected / unique	24573 / 8147 [R(int) = 0.0748]	22849 / 7728 [R(int) = 0.0735]
Completeness to theta	26.00 99.9 %	25.00 99.9 %
Absorption correction	Analytical	Analytical
Max. and min. transmission	0.7173 and 0.2678	0.3952 and 0.0818
Data / restraints / parameters	8147 / 1 / 415	7728 / 1 / 415
Goodness-of-fit on F^2	0.749	1.033
Final R indices [I>2sigma(I)]	R1 = 0.0417, wR2 = 0.0754	R1 = 0.0532, wR2 = 0.0853
R indices (all data)	R1 = 0.1177, wR2 = 0.0868	R1 = 0.1162, wR2 = 0.1018
Absolute structure parameter	0.002(8)	0.021(12)
Largest diff. peak and hole, e $Å^{-3}$	0.519 and -0.582	0.845 and -0.483

Table 3. Selected bond lengths and bond angles for MnL^{NEX}(TBC) from the X-ray crystallographic structures

Bond distances (Å)	***MnL^{NEC}(TBC)***	***MnL^{NEB}(TBC)***
Mn1-O3	1.881(4)	1.893(6)
Mn1-O1	1.898(4)	1.899(6)
Mn1-O2	2.023(4)	2.056(5)
Mn1-O4	2.039(4)	2.024(5)
Mn1-N2	2.212(5)	2.196(7)
Mn1-N1	2.292(5)	2.328(6)
Bond angles (°)		
O3-Mn1-O1	175.36(18)	174.6(2)
O3-Mn1-O2	91.21(18)	92.3(2)
O1-Mn1-O2	92.07(16)	92.1(2)
O3-Mn1-O4	82.92(17)	83.1(2)
O1-Mn1-O4	93.32(16)	93.3(2)
O2-Mn1-O4	99.02(16)	98.9(2)
O3-Mn1-N2	87.55(19)	87.5(3)
O1-Mn1-N2	95.91(18)	95.7(2)
O2-Mn1-N2	86.77(18)	86.7(2)
O4-Mn1-N2	168.93(17)	169.3(2)
O3-Mn1-N1	90.76(18)	89.8(2)
O1-Mn1-N1	86.83(16)	86.6(2)
O2-Mn1-N1	166.22(17)	165.7(2)
O4-Mn1-N1	94.76(16)	95.4(2)
N2-Mn1-N1	79.69(19)	79.3(2)

Table 4. Hydrogen bonds for MnL^{NEB}(TBC) [Å and º].

D-H...A	d(D-H)	d(H...A)	d(D...A)	<(DHA)
N3-H1N...O4[x,y,1+z]	0.91	2.04	2.916(6)	160
C10-H10B...O3	0.97	2.30	2.910(7)	120
C28-H28B...Br1	0.96	2.93	3.651(9)	133
C29-H29A...Cl4x,y,1+z]	0.97	2.79	3.622(7)	144
C29-H29B...O1[x,y,1+z]	0.97	2.32	3.196(8)	150

Table 5. Hydrogen bonds for **MnL^{NEC}(TBC)** [Å and º].

D-H...A	d(D-H)	d(H...A)	d(D...A)	<(DHA)
N3-H3N...O4	0.91	2.07	2.937(9)	159
C10-H10B...O3	0.97	2.29	2.91411)	121
C18-H18B...O1	0.96	2.54	3.045(12)	113
C27-H27B...Br5[x,y,-1+z]	0.97	2.87	3.620(10)	135
C28-H28C...O1	0.96	2.34	3.293(14)	174
C29-H29A...Br4	0.97	2.87	3.688(10)	142
C29-H29B...O1	0.97	2.38	3.245(10)	149

Table 6. Calculated parameters C, μ_{eff} and θ from the fit of the measured data.

Complex	C (emu K/mol)		μ_{eff}(BM)
MnL^{NEB}(TBC)	3.03	1.28	4.92
MnL^{NEC}(TBC)	1.90	1.30	3.89

Table 7. Oxygenative cleavage product of DTBC (**A**) by the $MnCl_2$/ H_2L^{NEC} system and its fragments monitored by GC/mass spectroscopy

Product	*m/z*
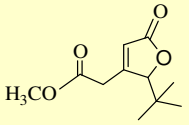	212
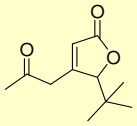	197
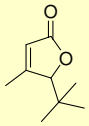	153
^{t}Bu	57

Table 8. Energies of the HOMO and LUMO spin α and β electrons for the complexes These HOMOs/LUMOs are all on the phenolate moieties of the complexes.

Molecule	*E(α HOMO)*	*E(α LUMO)*	*ΔE*	*E(β HOMO)*	*E(β LUMO)*	*ΔE*
FeL^{NEC}(TBC)	-0.10580	+0.02967	-0.13547	-0.10233	-0.02971	-0.07262
FeL^{NEB}(TBC)	-0.10789	0.02812	-0.13601	-0.10443	-0.03234	-0.07209
MnL^{NEC}(TBC)	-0.10795	-0.02125	-0.0867	-0.10842	0.01328	-0.1217
MnL^{NEB}(TBC)	-0.10983	-0.02366	-0.08617	-0.11078	0.01069	-0.12147